Published in final edited form as:
Eur J Nucl Med Mol Imaging. 2011 October ; 38(10): 1816–1823. doi:10.1007/s00259-011-1876-z.

Investigation on Tumor Hypoxia in Resectable Primary Prostate Cancer as Demonstrated by ^{18}F-FAZA PET/CT Utilizing Multi-Modality Fusion Techniques

Rita Garcia-Parra[1,2], **David Wood**[3], **Rajal B. Shah**[4], **Javed Siddiqui**[4], **Hero Hussain**[1], **Hyunjin Park**[1,5], **Timothy Desmond**[1], **Charles Meyer**[1], and **Morand Piert**[1]

[1]Department of Radiology, University of Michigan, USA

[2]Nuclear Medicine, University of Milan Bicocca, Monza, Italy

[3]Urology Department, University of Michigan, USA

[4]Pathology Department, University of Michigan, USA

[5]Deptartment of Biomedical Engineering, Gachon University of Medicine and Science, Incheon, S. Korea

Abstract

Purpose—As hypoxia is believed to play an important role in the development and progression of prostate cancer, we evaluated whether ^{18}F-labelled Fluoroazomycin Arabinoside (^{18}F-FAZA) would be useful to identify tumor hypoxia in resectable prostate cancer.

Methods—PET/CT was performed on 14 patients with untreated localized primary prostate cancer 3 hours post injection of approximately 390 MBq of ^{18}F-FAZA using forced diuresis to decrease radioactivity in the urinary bladder. Anatomical transpelvic coil and pre- and post-contrast 1.5 T MRI with endorectal coil were performed on the same day. Patients underwent radical prostatectomy and *ex-vivo* 3T MRI of the prostatectomy specimen within 14 days following *in-vivo* imaging. Imaging results were verified by whole mount histopathology plus tissue microarray (TMA) immunohistochemical (IHC) analysis for carbonic anhydrase IX (CAIX) and HIF-1α. Registration of *in-vivo* imaging with histology was achieved using mutual information software and performing *ex-vivo* MRI of the prostatectomy specimen and whole mount sectioning with block face photography as intermediate steps.

Results—Whole mount histology identified 43 tumor nodules, 19 of them larger than 1 ml as determined on coregistered volumes featuring ^{18}F-FAZA, MRI and histological 3D image information. None of these lesions was found to be positive for CAIX or visualized by ^{18}F-FAZA PET/CT while IHC for HIF-1α showed variable staining of tumor tissues. Accordingly, no correlation was found between ^{18}F-FAZA uptake and Gleason scores.

Conclusion—Our data based on ^{18}F-FAZA PET/CT and CAIX IHC do not support the presence of clinically relevant hypoxia in localized primary prostate cancer including high-grade disease. Activation of HIF-1α may be independent on tissue hypoxia in primary prostate cancer.

Corresponding author Morand Piert, M.D., Associate Professor of Radiology, University of Michigan Health System, Dept. of Radiology, Division of Nuclear Medicine, University Hospital B1G505C, 1500 E. Medical Center Drive, Ann Arbor, MI 48109-0028, USA, Tel. (734) 936 5388, FAX. (734) 936 8182, mpiert@umich.edu.

Conflict of interest
The authors declare that they have no conflict of interest.

Keywords

Hypoxia; Fluoroazomycin Arabinoside; 18F-FAZA; PET/CT; PET/MRI fusion; HIF-1α; CAIX; MIB-1/Ki67; Immunohistochemistry; Prostate cancer

Introduction

Hypoxia is thought to play an important role in the development and progression of prostate cancer. Evidence for hypoxia in human prostate cancer has been documented by both electrode measurements of tissue oxygen levels [1] and immunohistochemistry for the hypoxia-inducible factor HIF-1α [2]. Increasing levels of hypoxia have been associated with increasing clinical stage of prostate cancer, age [3] and predictors for biochemical failure [1] and radiation resistance [4–6].

Non invasive measurements of hypoxia have been performed using positron emission tomography (PET) with 1-α-D-(5-deoxy-5-[18F]-fluoroarabinofuranosyl)-2-nitroimidazole (^{18}F-FAZA) in several human cancers with suitable tumor-to-background ratios [7–11]. Nitroimidazole radiotracer uptake has been linked to treatment resistance of several cancers in preclinical [12] and clinical studies [13], indicating the potential for detection of hypoxia in radiation treatment of prostate cancer [14].

In order to assess the presence of hypoxia in primary prostate cancer, we used ^{18}FFAZA PET/CT correlating uptake measures with spatially coregistered for the established immunohistochemical (IHC) markers HIF-1α and carbonic anhydrase IX (CAIX), both frequently overexpressed in tumor hypoxia [15–18]. In many human malignancies including urological cancers, staining for CAIX has been found to be a predictor of poor prognosis [19–22]. Fusion of histology with ^{18}F-FAZA PET/CT measurements was made possible by a sophisticated fusion technique involving MRI as intermediate steps [23]. Registration errors for fusion of *in-vivo* imaging with histology involving specimen MRI were previously determined to be in the range of 2–4 mm, providing the necessary accuracy for spatial comparisons of volumetric PET data and pathology [24].

Materials and Methods

Patient Population

Fourteen males with untreated localized primary biopsy-proven adenocarcinoma of the prostate scheduled for prostatectomy were recruited. The mean patient age was 60.6 years (range 46 – 72 years) and the mean weight was 91.9 ± 10.4 kg (range 75–109 kg). Patients underwent prostate biopsies (6 samples from each lobe) within 16 weeks of enrolment. Inclusion criteria were 3 or more cores positive for a Gleason score ≥3+3 cancer from at least one lobe of the prostate. Patients with prior androgen ablation treatment, prostate biopsies performed less than 6 weeks before PET/MRI imaging, previous external radiation treatment of the pelvic region, any prior malignancies, active inflammatory bowel disease or evidence of prostatitis were excluded from this study.

Imaging

^{18}F-FAZA PET/CT was performed, within 14 days prior to radical prostatectomy (mean 7.9 ± 3.3 days, range 3–14 days), on a Siemens Biograph scanner. Patients were injected intravenously with 389 ± 17 MBq of ^{18}F-FAZA. About 15 minutes later, an IV infusion of 1000 ml NaCl 0.9% with 40 mg furosemide was administered to decrease radioactivity in the urinary bladder at the time of imaging. Patients were asked to drink additional water and

void their urinary bladder as frequently as possible. Three hours post injection, a limited body scan of the abdomen was performed. Iterative (OSEM) image reconstruction (Fourier-rebinning (FORE), 4 iterations, 8 subsets) with a 7 mm Gaussian filter resulted in $5.2\times5.2\times2.4$ mm^3 voxel dimension utilizing a low-dose CT without intravenous or oral contrast for attenuation correction [23].

In vivo anatomical MRI was performed for subsequent image coregistration with PET/CT on 1.5T field strength (Signa, General Electric, Milwaukee, USA) using an endorectal coil combined with a surface coil, and on 3T field strength (Achieva, Philips Healthcare, Best, The Netherlands) using a torso/cardiac 16 channel phased-array coil on the same day. Axial T2-weighted imaging on 3T was performed using a fast spin-echo sequence (Echo train length (ETL) = 15) and the following parameters: TR/TE: 2800/80 ms, FOV: 280 × 280 mm, matrix: 388 (frequency) × 307 (phase), slice thickness 3 mm without interslice gap, 28 slices total. On 1.5T, axial T2-weighted imaging was also performed using a FSE sequence (ETL 16) with the following parameters: TR/TE: 3050/120 ms, FOV: 140 × 140 mm, matrix 256 (frequency) × 194 (phase), slice thickness 3 mm without interslice gap, 28 slices total. Images were reconstructed in a voxel dimension of $0.31 \times 0.31 \times 4$ mm^3. Isotropic axial diffusion-weighted scans were performed on 1.5T using a single-shot Echo-Planar imaging sequence (EPI) with the following parameters: TR/TE:6000/65 ms, FOV 240 × 240 mm, matrix 128 × 128 (frequency × phase) reconstructed to a 256 × 256 matrix, slice thickness: 4 mm with no gap, b-values: 0 and 800 s/mm^2 [25]. Patients underwent radical prostatectomy and *ex-vivo* of the prostatectomy specimen was performed on 3T field strength within 14 days following the *in-vivo* imaging.

Image Coregistration

Image registration was performed using a standard mutual information objective function with thin-plate spline deformation [26]. Accurate image volume registration involving histology was performed as described earlier [24, 27]. Briefly, our approach separated the difficult direct registration of histology and *in-vivo* imaging (PET, MRI) into achievable subregistration tasks involving intermediate *ex-vivo* modalities like block face photography and specimen MRI, which was performed 2–3 days after prostatectomy. Block phase photographs and histology were volumetrically stacked to compute the final registration between our reference space (T2-weighted MR) and whole mount histology.

Histological Assessment and Tissue Microarray Construction

Details of the histological assessment are available in the literature [23]. Briefly, fresh prostates were fixed in 10% neutral formalin and sectioned at 3-mm intervals using whole-mount technique [28]. Tumor maps were generated for each whole-mount slice to determine individual tumor foci [29]. Each focus was assigned a primary and secondary Gleason grade and staged according to the 1998 AJCC staging guidelines [30]. A TMA representing a total of 43 tumor foci was constructed from 14 prostatectomy specimens. Three cores were taken from each representative tumor focus as well as from benign control tissues to construct the tissue microarray.

The formalin-fixed, paraffin-embedded whole mount histopathology was evaluated for the presence of carboanhydrase IX (CAIX, Novus), the hypoxia inducible factor-1α (HIF-1α, Chemicon) and the proliferation marker MIB-1/Ki-67 (Dako) using TMA analysis. Each antibody was individually evaluated using varying incubation times, antigen retrieval protocols, and dilution series, with final adjustments and optimization being done on test arrays before final testing on our TMAs. All staining protocols have been published previously in detail [31, 32]. A single pathologist (R.S.), blinded to clinical outcome and imaging results performed the quantitative assessment of protein expression. The extent of

expression ("staining frequency") was recorded as percentage of the entire tumor sample that stained positive with consideration of staining intensity.

Image Analysis

In order to compare *in-vivo* imaging results with histology (local Gleason score, HIF-1α, MIB-1/Ki-67 and CAIX labeling indices), volumes of interest (VOI) were defined on coregistered consecutive pathological sections contouring lesion borders individually. In each patient, at least one standardized VOI (1.5 ml) could be defined for non-malignant tissue in the peripheral zone and central gland. All VOI were transferred into coregistered ^{18}F-FAZA images scaled to the standardized uptake value (SUV). PET imaging results were normalized by benign prostate tissue before further analysis. We calculated the mean tumor-to-benign background ($T_{(mean)}$/B) and the maximum tumor-to-normal ($T_{(max)}$/B) ratio using non-malignant contra-lateral tissue as reference. Tumor uptake was normalized according to location, thus peripheral zone tumors were normalized by non-malignant contra-lateral peripheral zone tissue.

Statistics

Results are expressed as mean values of parameters ±SD. Statistical analysis was performed as described earlier [23]. Briefly, parameters were compared by means of 1-way ANOVA using the tumor volume as weighting factor, including tests for homogeneity of group variances using the Bartlett test. Group differences were assessed using the Wilcoxon rank sign test. Parameters were correlated using a nonparametric test (Spearman rank correlation). $P < 0.05$ was considered statistically significant. Statistical tests were performed with the JMP statistical software package (SAS).

Results

As summarized in Table 1, patients were staged T2b to T3b at pathology with a mean PSA of 8.1 ±.4.2 ng/mL (range 2.2 – 17.9). The weight of the prostate specimen ranged from 49.4 to 64.5 g.

Whole mount histology identified 43 tumor nodules (volume range 0.03–12.6 ml), 19 of them larger than 1 ml as determined on coregistered volumes featuring ^{18}F-FAZA, MRI and histological 3D image information. Individual Gleason scores ranged from 3+2 to 4+4, while the Gleason score of the largest lesion per patient varied between 3+4 and 4+4.

A relative uniform distribution of ^{18}F-FAZA uptake was noted within the non-malignant prostate tissues. The mean ^{18}F-FAZA SUV of the non-malignant central gland (mean SUV 3.0 ± 2.8) was slightly, but not significantly higher than the respective benign peripheral gland (mean SUV, 2.4 ± 2.2). More importantly, none of the tumor lesions identified on histology showed increased ^{18}F-FAZA uptake (Figure 1 and 2), thus even high grade prostate cancers with Gleason ≥ 4+3 and positive for MIB-1/Ki67 did not exhibit detectable levels of hypoxia.

The immunohistochemical marker scores for MIB-1/Ki67 and HIF-1α obtained from prostate cancer lesions were not significantly correlated. MIB-1/Ki67 showed significantly increased scores in high-grade tumors with a Gleason ≥ 4+3 compared to Gleason ≤ 3+4 and lower ($p < 0.05$). Positive HIF-1α staining was noted in all Gleason categories without preference for a particular Gleason grade (Figure 3). Tumor volume was not significantly correlated with HIF-1α staining. None of the prostate cancer lesions displayed positive staining for CAIX.

Benign prostatic tissue did not show positive staining for MIB-1/Ki67 or CAIX. However, in one patient, positive HIF-1α staining was observed in hyperplastic benign tissues.

Discussion

Recent clinical studies with ^{18}F-FAZA showed favorable imaging characteristics of this hypoxia imaging agent, given good imaging properties with acceptable T/B ratios, for squamous cell carcinoma of the head and neck (HNSCC), small-cell lung cancer (SCLC) or non-small-cell lung cancer (NSCLC), malignant lymphoma, and high-grade gliomas [33, 34]. Even though literature suggests a role of hypoxia in the development and progression of prostate cancer, our data do not support a major role of ^{18}F-FAZA PET imaging in resectable primary prostate cancer, even in high-grade disease

What are the implications of these findings for prostate cancer? First, we consider it quite unlikely that none of the 14 subjects lacked hypoxia in prostate cancer nodules purely by chance. While tumor size is not the most important determinant for the presence of tumor hypoxia, it is certainly true that larger tumor masses are more likely to be (at least partially) hypoxic compared to smaller malignancies. Five patients had tumor volumes greater than 4 cm^3, one of them was as large as 12.6 cm^3, a size range expected to develop some degree of tumor hypoxia.

What is the evidence for hypoxia in primary prostate cancer? Oxygen tension has been measured with needle electrode systems in few series. When Movas et al. investigated patients undergoing brachytherapy or prostatectomy for prostate cancer, a clear significant difference of the tissue oxygen tensions was found between prostate gland tissue and muscle, while intraprostatic oxygen tension varied to a much lesser degree. Prostatic oxygenation was dependent on the type of anesthesia and disease stage, but a comparison of benign vs. malignant prostate tissue was not attempted [1, 3]. A second study employing needle electrode measurements, no significant difference was found between the oxygen tension of normal prostate tissue and foci of prostate cancer [35]. Similarly, in this study we did not observe a significant difference between the mean or maximum SUV of ^{18}F-FAZA in prostate cancer compared to benign prostatic tissues, even when only larger tumors (volume above 2 cm^3) were included in the analysis.

Using immunohistochemistry methods, many studies showed overexpression of HIF-1α in human specimens of prostate cancer. Nuclear staining is commonly identified in the majority of prostate cancer samples [17], but to a significant portion also in intraepithelial neoplasm and benign prostate hyperplasia, while no detectable expression is generally noted for normal tissues [36]. Supporting our findings, expression of the HIF-1α molecule is already seen at early stages of prostate cancer development [18]. In human prostate cancer as well as other cancers, HIF-1α overexpression may however be induced by other factors than tissue hypoxia [37, 38]. Not surprisingly, little evidence suggests a significant correlation between IHC HIF-1α expression and clinical outcome or prognostic factors [22, 39].

Upregulation of CAIX is a consequence of HIF-1α stabilization [40]. CAIX overexpression has been associated with tumor cell hypoxia and has been found to correlate with poor outcome for many malignancies [21], including cervical squamous carcinoma [41], esophageal and gastric adenocarcinomas [42], breast cancer [43], and urologic cancers [19]. CAIX plays an important role in maintaining intracellular pH-balance counteracting hypoxia-induced acidosis, thereby promoting cell survival and growth [44]. Very few normal tissues express significant amounts of CAIX, so that positive staining in now an established marker of tumor hypoxia and a clinical indicator of aggressive cancers [45].

Expression of CAIX in prostate cancer is controversial. Several studies confirmed the presence of CAIX in human prostate cancer cell lines [15, 46, 47]. In a recent pilot study of five men with prostate cancer, biopsies were stained for CAIX, HIF-1α and GLUT-1, showing an overexpression of HIF-1α and GLUT-1 in all patients, while CAIX was upregulated in only one patient with very low tissue pO_2 values (1.4 mmHg as determined by oxygen needle measurements) [20]. Similar findings were reported by Smyth et al., who observed only occasional cell staining for CAIX while HIF-1α staining was generally positive in prostate cancer [48]. Our results, a lack of CAIX expression with positive HIF-1α staining in many prostate cancer lesions independent on Gleason scores, are further supporting the results of Smyth et al.

As CAIX upregulation is generally accepted to be the consequence of hypoxia-induced HIF-1α stabilization [40, 44] and since intracellular hypoxia is associated with disturbances in pH regulation causing intracellular acidosis [45], our data suggest that the overexpression of HIF-1α in primary prostate cancer is predominantly independent on intracellular hypoxia. Thus, our data support earlier findings regarding alternative mechanisms for HIF-1α stabilization in prostate cancer [38], which ultimately may be linked to the ability of androgens to promote angiogenesis through activation of HIF-1α in androgen-sensitive prostate cancer [49].

In the light of negative ^{18}F-FAZA accumulation in primary prostate cancer, our results suggest that IHC for CAIX, and not HIF-1α, may be a better indicator for the true oxygenation status of primary prostate cancer. Despite the lack of detectable hypoxia in primary prostate cancer, our data appear to be of clinical relevance as modifications to radiation treatment planning based on hypoxia imaging have been proposed for prostate cancer [50].

Conclusion

In many human cancers, nitroimidazole tracers such as ^{18}F-FAZA have consistently been successful in identifying tissue hypoxia.. However, our data indicate that clinically relevant hypoxia is unlikely to exist in localized primary prostate cancer including high-grade disease to a degree that would be detectable with ^{18}F-FAZA PET/CT or IHC with CAIX. In addition, HIF-1α cannot be recommended as IHC marker of hypoxia as its expression in the prostate seems to be independent on hypoxia.

In the current study, evaluation of hypoxia in prostate cancer was limited to primary prostate cancer undergoing surgical resection. However, it remains to be determined whether significant hypoxia might be present in advanced (unresectable) local, recurrent or metastatic prostate cancer.

Acknowledgments

This research is supported by P01CA87634 and P50CA069568.

References

1. Movsas B, Chapman JD, Hanlon AL, Horwitz EM, Greenberg RE, Stobbe C, et al. Hypoxic prostate/muscle pO2 ratio predicts for biochemical failure in patients with prostate cancer: preliminary findings. Urology. 2002; 60:634–639. [PubMed: 12385924]
2. Lekas A, Lazaris AC, Deliveliotis C, Chrisofos M, Zoubouli C, Lapas D, et al. The expression of hypoxia-inducible factor-1alpha (HIF-1alpha) and angiogenesis markers in hyperplastic and malignant prostate tissue. Anticancer Res. 2006; 26:2989–2993. [PubMed: 16886625]

3. Movsas B, Chapman JD, Greenberg RE, Hanlon AL, Horwitz EM, Pinover WH, et al. Increasing levels of hypoxia in prostate carcinoma correlate significantly with increasing clinical stage and patient age: an Eppendorf pO(2) study. Cancer. 2000; 89:2018–2024. [PubMed: 11064360]
4. Stewart GD, Ross JA, McLaren DB, Parker CC, Habib FK, Riddick AC. The relevance of a hypoxic tumour microenvironment in prostate cancer. BJU Int. 2009; 105:8–13. [PubMed: 19889065]
5. Carnell DM, Smith RE, Daley FM, Saunders MI, Bentzen SM, Hoskin PJ. An immunohistochemical assessment of hypoxia in prostate carcinoma using pimonidazole: implications for radioresistance. Int J Radiat Oncol Biol Phys. 2006; 65:91–99. [PubMed: 16563659]
6. Arabi M, Piert M. Hypoxia PET/CT imaging: implications for radiation oncology. Q J Nucl Med Mol Imaging. 2010; 54:500–509. [PubMed: 20927017]
7. Souvatzoglou M, Grosu AL, Roper B, Krause BJ, Beck R, Reischl G, et al. Tumour hypoxia imaging with [18F]FAZA PET in head and neck cancer patients: a pilot study. Eur J Nucl Med Mol Imaging. 2007; 34:1566–1575. [PubMed: 17447061]
8. Postema EJ, McEwan AJ, Riauka TA, Kumar P, Richmond DA, Abrams DN, et al. Initial results of hypoxia imaging using 1-alpha-D: -(5-deoxy-5-[(18)F]-fluoroarabinofuranosyl)-2-nitroimidazole ((18)F-FAZA). Eur J Nucl Med Mol Imaging. 2009
9. Grosu AL, Souvatzoglou M, Roper B, Dobritz M, Wiedenmann N, Jacob V, et al. Hypoxia Imaging With FAZA-PET and Theoretical Considerations With Regard to Dose Painting for Individualization of Radiotherapy in Patients With Head and Neck Cancer. Int J Radiat Oncol Biol Phys. 2007; 69:541–551. [PubMed: 17869667]
10. Piert, M. Hypoxia Imaging. In: Wahl, RL., editor. Principles and Practices of PET and PET/CT. 2. ed. Lippincott Williams & Wilkins; 2008. in press
11. Krause BJ, Beck R, Souvatzoglou M, Piert M. PET and PET/CT studies of tumor tissue oxygenation. Q J Nucl Med Mol Imaging. 2006; 50:28–43. [PubMed: 16557202]
12. Beck R, Roper B, Carlsen JM, Huisman MC, Lebschi JA, Andratschke N, et al. Pretreatment 18F-FAZA PET predicts success of hypoxia-directed radiochemotherapy using tirapazamine. J Nucl Med. 2007; 48:973–980. [PubMed: 17536108]
13. Eschmann SM, Paulsen F, Reimold M, Dittmann H, Welz S, Reischl G, et al. Prognostic impact of hypoxia imaging with ^{18}F-misonidazole PET in non-small cell lung cancer and head and neck cancer before radiotherapy. J Nucl Med. 2005; 46:253–260. [PubMed: 15695784]
14. Beer AJ, Grosu AL, Carlsen J, Kolk A, Sarbia M, Stangier I, et al. [18F]galacto-RGD positron emission tomography for imaging of alphavbeta3 expression on the neovasculature in patients with squamous cell carcinoma of the head and neck. Clin Cancer Res. 2007; 13:6610–6616. [PubMed: 18006761]
15. Li Y, Wang H, Oosterwijk E, Selman Y, Mira JC, Medrano T, et al. Antibody-specific detection of CAIX in breast and prostate cancers. Biochem Biophys Res Commun. 2009; 386:488–492. [PubMed: 19538935]
16. Jans J, van Dijk JH, van Schelven S, van der Groep P, Willems SH, Jonges TN, et al. Expression and localization of hypoxia proteins in prostate cancer: prognostic implications after radical prostatectomy. Urology. 2010; 75:786–792. [PubMed: 19854473]
17. Boddy JL, Fox SB, Han C, Campo L, Turley H, Kanga S, et al. The androgen receptor is significantly associated with vascular endothelial growth factor and hypoxia sensing via hypoxia-inducible factors HIF-1a, HIF-2a, and the prolyl hydroxylases in human prostate cancer. Clin Cancer Res. 2005; 11:7658–7663. [PubMed: 16278385]
18. Zhong H, De Marzo AM, Laughner E, Lim M, Hilton DA, Zagzag D, et al. Overexpression of hypoxia-inducible factor 1alpha in common human cancers and their metastases. Cancer Res. 1999; 59:5830–5835. [PubMed: 10582706]
19. Ord JJ, Agrawal S, Thamboo TP, Roberts I, Campo L, Turley H, et al. An investigation into the prognostic significance of necrosis and hypoxia in high grade and invasive bladder cancer. J Urol. 2007; 178:677–682. [PubMed: 17574616]
20. Chopra S, Foltz WD, Milosevic MF, Toi A, Bristow RG, Menard C, et al. Comparing oxygen-sensitive MRI (BOLD R2*) with oxygen electrode measurements: a pilot study in men with prostate cancer. Int J Radiat Biol. 2009; 85:805–813. [PubMed: 19728195]

21. Potter C, Harris AL. Hypoxia inducible carbonic anhydrase IX, marker of tumour hypoxia, survival pathway and therapy target. Cell Cycle. 2004; 3:164–167. [PubMed: 14712082]
22. Vergis R, Corbishley CM, Norman AR, Bartlett J, Jhavar S, Borre M, et al. Intrinsic markers of tumour hypoxia and angiogenesis in localised prostate cancer and outcome of radical treatment: a retrospective analysis of two randomised radiotherapy trials and one surgical cohort study. Lancet Oncol. 2008; 9:342–351. [PubMed: 18343725]
23. Piert M, Park H, Khan A, Siddiqui J, Hussain H, Chenevert T, et al. Detection of aggressive primary prostate cancer with 11C-choline PET/CT using multimodality fusion techniques. J Nucl Med. 2009; 50:1585–1593. [PubMed: 19759109]
24. Park H, Piert MR, Khan A, Shah R, Hussain H, Siddiqui J, et al. Registration methodology for histological sections and in vivo imaging of human prostate. Acad Radiol. 2008; 15:1027–1039. [PubMed: 18620123]
25. Chenevert, TL.; Welsh, RC. Diffusion Tensor MR Imaging. In: Haacke, EM., editor. Current Protocols in Magnetic Resonance Imaging. Wiley Online Library; 2004.
26. Meyer CR, Boes JL, Kim B, Bland PH, Zasadny KR, Kison PV, et al. Demonstration of accuracy and clinical versatility of mutual information for automatic multimodality image fusion using affine and thin-plate spline warped geometric deformations. Med Image Anal. 1997; 1:195–206. [PubMed: 9873906]
27. Park H, Meyer CR, Wood D, Khan A, Shah R, Hussain H, et al. Validation of Automatic Target Volume Definition as Demonstrated for (11)C-Choline PET/CT of Human Prostate Cancer Using Multi-Modality Fusion Techniques. Acad Radiol. 2010; 17:614–623. [PubMed: 20188602]
28. Shah R, Bassily N, Wei J, Mucci NR, Montie JE, Sanda MG, et al. Benign prostatic glands at surgical margins of radical prostatectomy specimens: frequency and associated risk factors. Urology. 2000; 56:721–725. [PubMed: 11068287]
29. Mehra R, Han B, Tomlins SA, Wang L, Menon A, Wasco MJ, et al. Heterogeneity of TMPRSS2 gene rearrangements in multifocal prostate adenocarcinoma: molecular evidence for an independent group of diseases. Cancer Res. 2007; 67:7991–7995. [PubMed: 17804708]
30. Fleming, ID.; Cooper, JS.; Henson, DE. AJCC cancer staging manual. 5th. ed.. Philadelphia: Lippincott, Raven; 1998.
31. May M, Siegsmund M, Hammermann F, Loy V, Gunia S. Prognostic significance of proliferation activity and neuroendocrine differentiation to predict treatment failure after radical prostatectomy. Scand J Urol Nephrol. 2007; 41:375–381. [PubMed: 17853019]
32. Shah R, Mucci NR, Amin A, Macoska JA, Rubin MA. Postatrophic hyperplasia of the prostate gland: neoplastic precursor or innocent bystander? Am J Pathol. 2001; 158:1767–1773. [PubMed: 11337374]
33. Postema EJ, McEwan AJ, Riauka TA, Kumar P, Richmond DA, Abrams DN, et al. Initial results of hypoxia imaging using 1-alpha-D: -(5-deoxy-5-[18F]-fluoroarabinofuranosyl)-2-nitroimidazole (18F-FAZA). Eur J Nucl Med Mol Imaging. 2009; 36:1565–1573. [PubMed: 19430784]
34. Souvatzoglou M, Grosu AL, Roper B, Krause BJ, Beck R, Reischl G, et al. Tumour hypoxia imaging with [(18)F]FAZA PET in head and neck cancer patients: a pilot study. Eur J Nucl Med Mol Imaging. 2007; 34:1566–1575. [PubMed: 17447061]
35. Parker C, Milosevic M, Toi A, Sweet J, Panzarella T, Bristow R, et al. Polarographic electrode study of tumor oxygenation in clinically localized prostate cancer. Int J Radiat Oncol Biol Phys. 2004; 58:750–757. [PubMed: 14967430]
36. Du Z, Fujiyama C, Chen Y, Masaki Z. Expression of hypoxia-inducible factor 1alpha in human normal, benign, and malignant prostate tissue. Chin Med J (Engl). 2003; 116:1936–1939. [PubMed: 14687488]
37. Tanaka H, Yamamoto M, Hashimoto N, Miyakoshi M, Tamakawa S, Yoshie M, et al. Hypoxia-independent overexpression of hypoxia-inducible factor 1alpha as an early change in mouse hepatocarcinogenesis. Cancer Res. 2006; 66:11263–11270. [PubMed: 17145871]
38. Banham AH, Boddy J, Launchbury R, Han C, Turley H, Malone PR, et al. Expression of the forkhead transcription factor FOXP1 is associated both with hypoxia inducible factors (HIFs) and the androgen receptor in prostate cancer but is not directly regulated by androgens or hypoxia. Prostate. 2007; 67:1091–1098. [PubMed: 17477366]

39. Mabjeesh NJ, Amir S. Hypoxia-inducible factor (HIF) in human tumorigenesis. Histol Histopathol. 2007; 22:559–572. [PubMed: 17330811]
40. Narita T, Yin S, Gelin CF, Moreno CS, Yepes M, Nicolaou KC, et al. Identification of a novel small molecule HIF-1alpha translation inhibitor. Clin Cancer Res. 2009; 15:6128–6136. [PubMed: 19789328]
41. Loncaster JA, Harris AL, Davidson SE, Logue JP, Hunter RD, Wycoff CC, et al. Carbonic anhydrase (CA IX) expression, a potential new intrinsic marker of hypoxia: correlations with tumor oxygen measurements and prognosis in locally advanced carcinoma of the cervix. Cancer Res. 2001; 61:6394–6399. [PubMed: 11522632]
42. Driessen A, Landuyt W, Pastorekova S, Moons J, Goethals L, Haustermans K, et al. Expression of carbonic anhydrase IX (CA IX), a hypoxia-related protein, rather than vascular-endothelial growth factor (VEGF), a pro-angiogenic factor, correlates with an extremely poor prognosis in esophageal and gastric adenocarcinomas. Ann Surg. 2006; 243:334–340. [PubMed: 16495697]
43. Trastour C, Benizri E, Ettore F, Ramaioli A, Chamorey E, Pouyssegur J, et al. HIF-1alpha and CA IX staining in invasive breast carcinomas: prognosis and treatment outcome. Int J Cancer. 2007; 120:1451–1458. [PubMed: 17245699]
44. Chiche J, Ilc K, Laferriere J, Trottier E, Dayan F, Mazure NM, et al. Hypoxia-inducible carbonic anhydrase IX and XII promote tumor cell growth by counteracting acidosis through the regulation of the intracellular pH. Cancer Res. 2009; 69:358–368. [PubMed: 19118021]
45. Swietach P, Hulikova A, Vaughan-Jones RD, Harris AL. New insights into the physiological role of carbonic anhydrase IX in tumour pH regulation. Oncogene. 2010; 29:6509–6521. [PubMed: 20890298]
46. Delacruz J, Mikulski R, Tu C, Li Y, Wang H, Shiverick KT, et al. Detecting extracellular carbonic anhydrase activity using membrane inlet mass spectrometry. Anal Biochem. 2010; 403:74–78. [PubMed: 20417171]
47. Anai S, Shiverick K, Medrano T, Nakamura K, Goodison S, Brown BD, et al. Downregulation of BCL-2 induces downregulation of carbonic anhydrase IX, vascular endothelial growth factor, and pAkt and induces radiation sensitization. Urology. 2007; 70:832–837. [PubMed: 17991582]
48. Smyth LG, O'Hurley G, O'Grady A, Fitzpatrick JM, Kay E, Watson RW. Carbonic anhydrase IX expression in prostate cancer. Prostate Cancer Prostatic Dis. 2010; 13:178–181. [PubMed: 20038959]
49. Boddy JL, Fox SB, Han C, Campo L, Turley H, Kanga S, et al. The androgen receptor is significantly associated with vascular endothelial growth factor and hypoxia sensing via hypoxia-inducible factors HIF-1a, HIF-2a, and the prolyl hydroxylases in human prostate cancer. Clinical cancer research : an official journal of the American Association for Cancer Research. 2005; 11:7658–7663. [PubMed: 16278385]
50. John SS, Zietman AL, Shipley WU, Harisinghani MG. Newer imaging modalities to assist with target localization in the radiation treatment of prostate cancer and possible lymph node metastases. Int J Radiat Oncol Biol Phys. 2008; 71:S43–S47. [PubMed: 18406936]

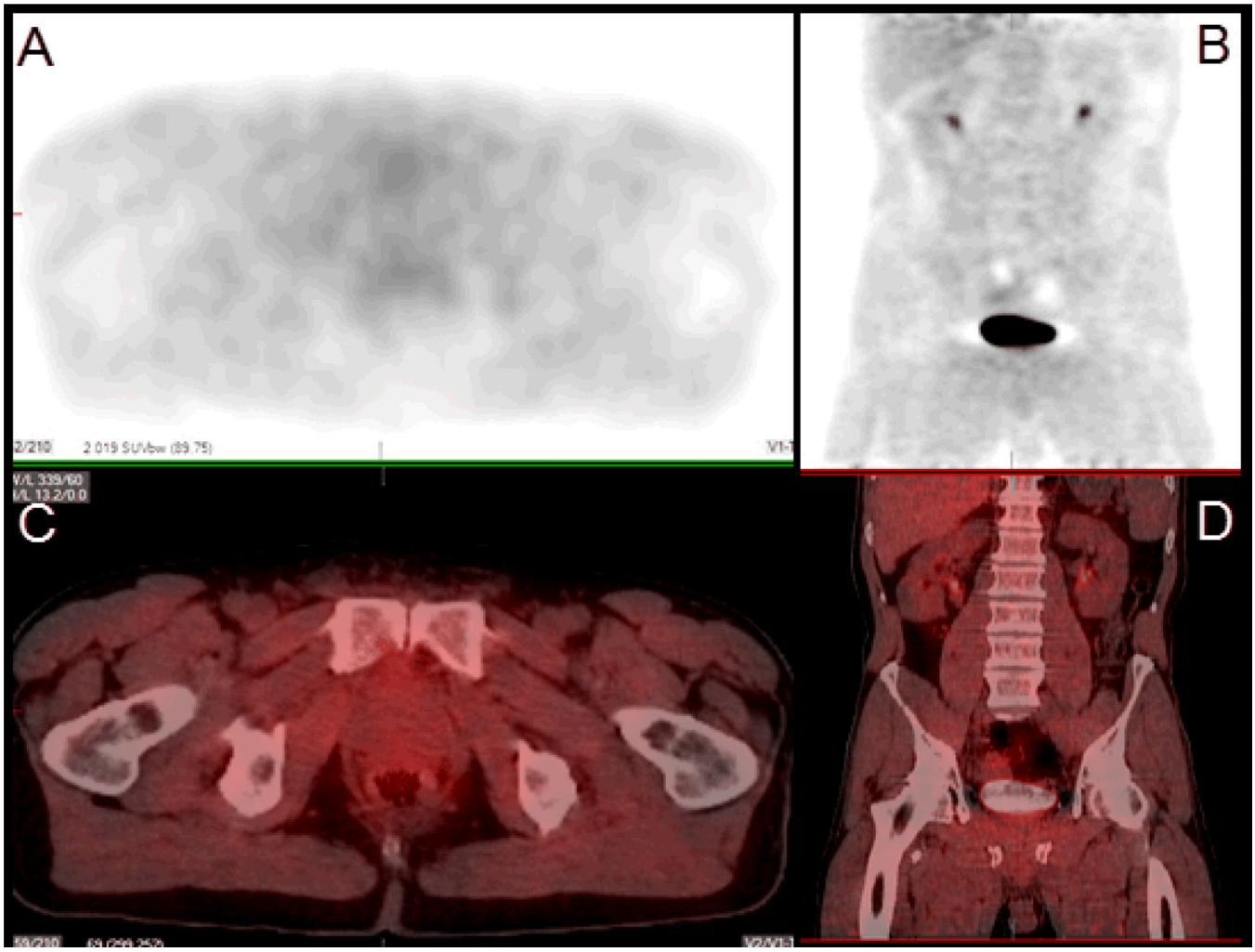

Figure 1.
Transaxial (A) and coronal (C) ^{18}F-FAZA PET/CT with respective fusion imaging (B, D) of a 7.8 ml volume tumor located in the peripheral zone on both sides of the gland. No increased ^{18}F-FAZA uptake is noted visually.

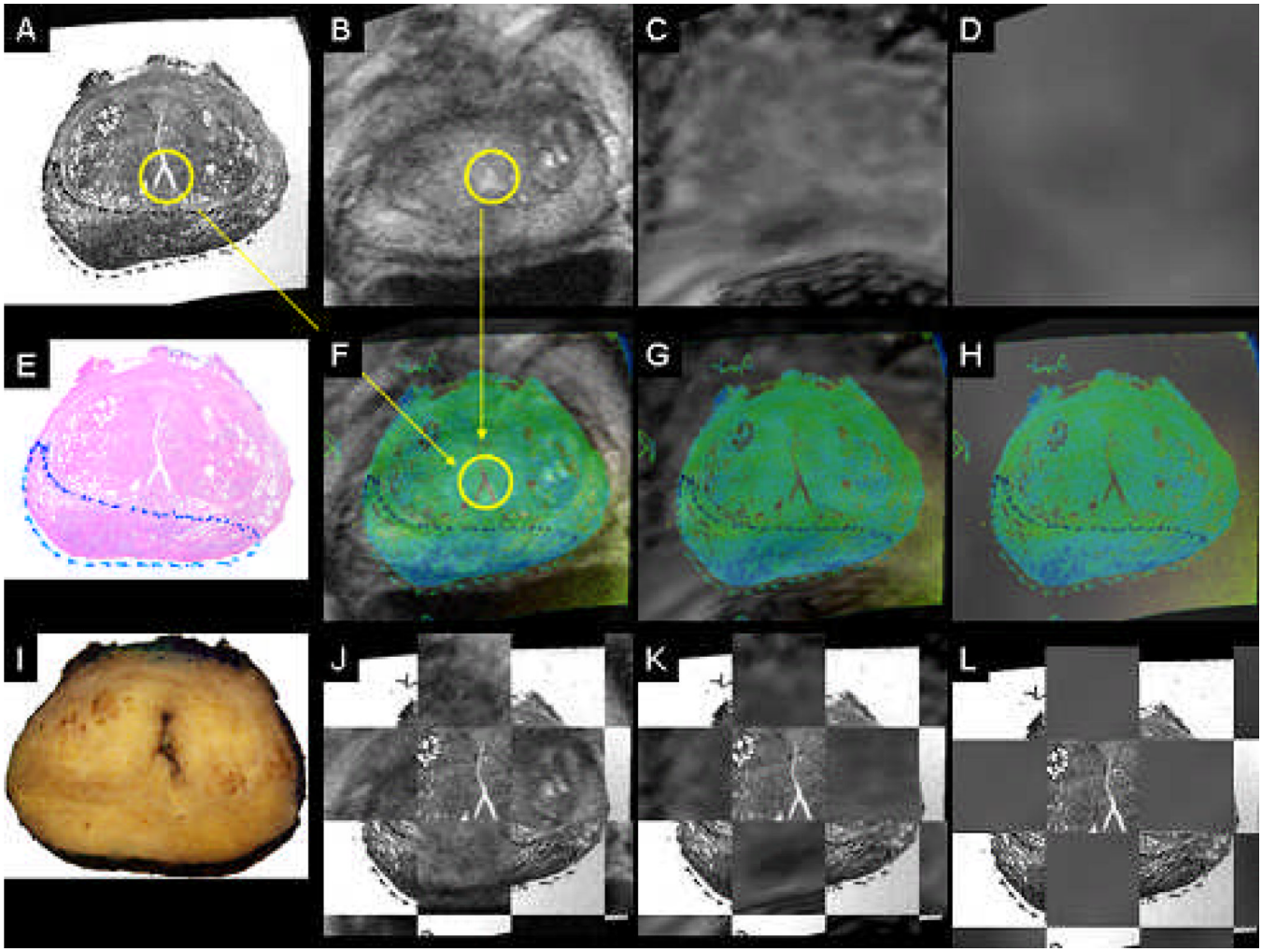

Figure 2.
Coregistered whole mount HE histology (A,E), *in-vivo* T2 MRI reference space (B), coregistered diffusion-weighted MRI (C), coregistered ^{18}F-FAZA PET/CT (D), coregistered color-coded histology and respective *in-vivo* imaging (F-H), block face photograph (I), coregistered color-coded histology and *in-vivo* imaging as checkerbox (J-L). Same patient as in Figure 1.

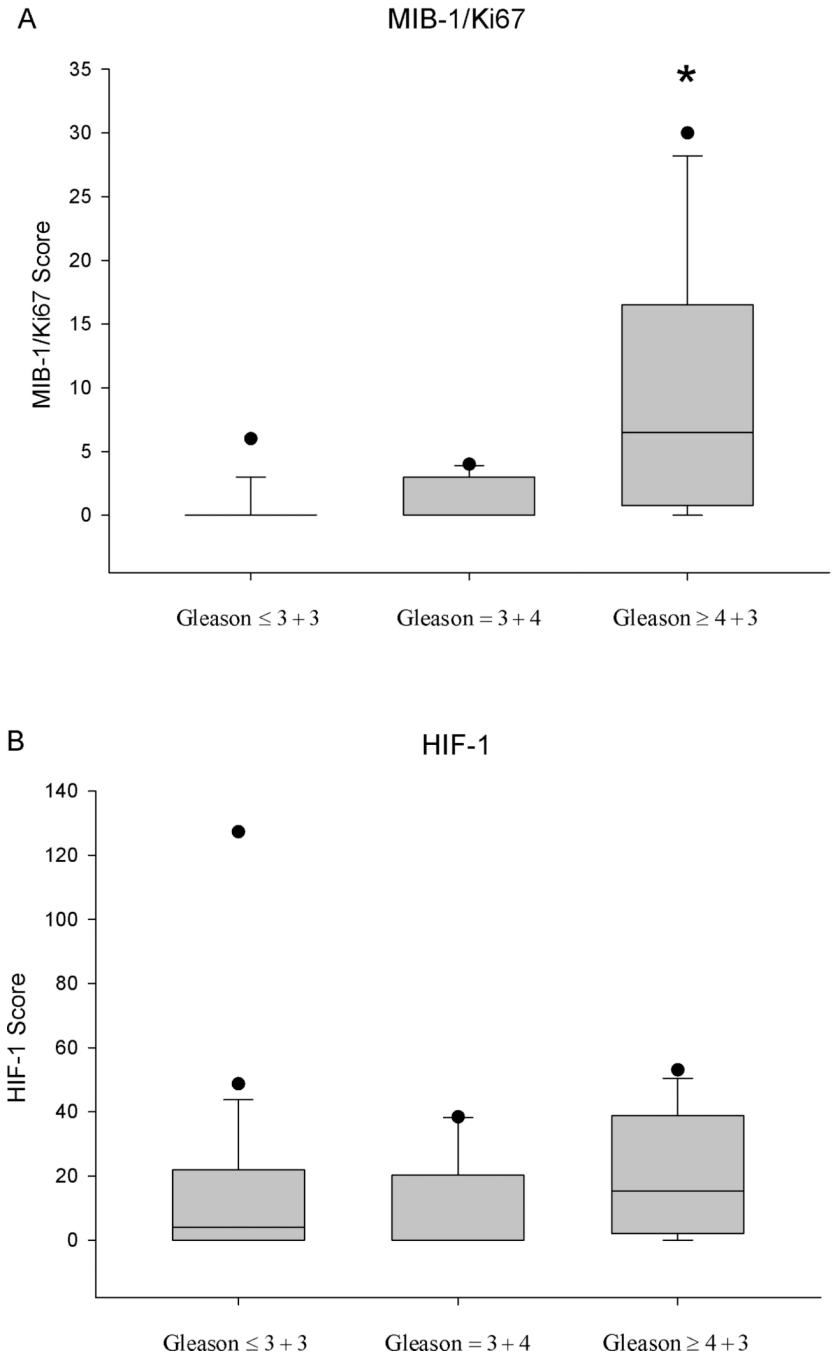

Figure 3.

Distribution of MIB-1/Ki67 (A) and HIF-1α (B) scores in various Gleason categories. * $p < 0.05$ Gleason ≥ 4+3 vs. Gleason ≤ 3+4 and lower disease.

Table 1

Patient Characteristics, Pathology and ^{18}F-FAZA Uptake Measures

Patient Number	Age (y)	^{18}F-FAZA injected activity (MBq)	PSA (ng/mL)	Prostate weight (g)	T-Stage	Highest Gleason Score	Tumor ^{18}F-FAZA SUV		Normal tissue Mean ^{18}F-FAZA SUV	
							Mean	Max	Peripheral	Central
1	62	384.8	13.0	46.1	T2b	4 + 3	2.8	3.9	2.7	2.7
2	72	409.6	8.7	40.9	T3a	3 + 4	0.9	1.1	0.9	1.0
3	60	407.0	8.5	45.1	T3a	4 + 3	2.6	5.6	3.4	1.4
4	56	399.6	7.1	52.8	T2b	4 + 3	1.4	1.8	1.2	0.8
5	59	407.7	12.1	49.1	T3b	4 + 4	1.0	2.5	1.0	0.9
6	59	388.5	17.9	63.0	T3b	4 + 4	0.4	0.6	0.7	0.5
7	64	347.8	2.2	64.5	T2b	3 + 4	1.8	4.7	1.7	1.9
8	66	383.0	5.9	41.2	T3a	4 + 3	4.2	8.8	2.3	3.4
9	67	399.6	3.9	43.8	T2b	4 + 3	2.7	3.1	3.1	3.1
10	64	381.1	10.2	47.7	T3b	4 + 3	4.7	8.0	4.3	4.9
11	55	370.0	4.6	41.7	T3a	3 + 4	1.6	4.9	1.1	6.3
12	63	395.9	4.4	44.9	T2b	4 + 3	5.2	14.1	2.3	2.1
13	46	395.9	6.9	39.7	T2b	3 + 4	2.7	7.2	1.6	3.1
14	56	386.7	8.2	45.4	T3a	4 + 3	0.5	0.6	0.4	0.5
Mean	60.6	389.8	8.1	47.6			2.3	4.8	1.9	2.3
SD	6.3	16.6	4.2	7.7			1.5	3.8	1.1	1.7

Eur J Nucl Med Mol Imaging. Author manuscript; available in PMC 2012 January 17.